# Simultaneous Homographic and Comparametric Alignment of Multiple Exposure-Adjusted Pictures of the Same Scene

Frank M. Candocia, *Member, IEEE*

***Abstract*—An approach is presented that can simultaneously align multiple exposure-adjusted pictures of the same scene both in their spatial coordinates as well as in their pixel values. The approach is featureless and produces an image mosaic at a common spatial and exposure reference and also addresses the misalignment problem common to methods that compose mosaics from only pair-wise registered image pairs. The objective function considered minimizes the sum of the collective variance over pixels of a global coordinate grid on which to create the final image. The models employed relate images spatially by homographic transformations and tonally by comparametric functions. The importance of performing joint spatial and tonal registration on exposure-adjusted images is emphasized by providing two examples in which spatial-only registration fails. A discussion describing the performance between pair-wise and simultaneous registration under both spatial-only and joint registration procedures is provided.**

***Index Terms*—Comparametric equation, domain and range registration, dynamic range map, exposure adjustment, homography, perspective projection, simultaneous alignment.**

## I. Introduction

IMAGE registration is increasingly being applied in a variety of diverse fields. Its been applied to the creation of virtual environments [1], [2] to be used in applications as tele-shopping, tele-realty and tele-travel. It has found use in the creation of large terrestrial mosaics from images gathered from aircraft and satellites [3]. In medical applications it has served for the purposes of planning and evaluation of surgical and radiotherapeutical procedures [4]. It has also been used in such problems as image resolution increase [5], depth extraction [6], video indexing [7] and video compression [8] to name a few.

An important factor to obtaining accurately registered images is the use of models that well describe the transformation between images. There have been various models used to describe the relations amongst the spatial coordinates, i.e., domain, of a set of images as well as amongst the pixel values, i.e., range, of the image functions considered [9]. Spatial coordinate transformations have typically accounted for a variety of linear mappings such as translational, rotational, affine or homographic mappings [10]–[12]. They have also been more complex and involved optical flow calculations [13] and the modeling of lens distortion [14]. These domain transformations are typically determined using either direct [15] or feature-based [16] methods. The registration of images tonally has seen work that models a camera's response function so that multiple images of a static scene, captured at different exposure settings, can been used to create high dynamic range maps whose resolution is greater than the typical 8 bits/pixel/channel [17]–[21]. Knowledge of this exposure difference has also been used to create range images where all objects in the scene are properly exposed [17], [22], [23]. The registration of images in both domain and range has resulted in work in which spatially varying optical filters have been attached to a camera so that, as the camera moves about a scene, points in the scene can be multiply imaged at different exposure settings [24], [25]. In this way, a mosaic of a scene can be created that also exhibits increased dynamic range. This joint registration has also been performed on images captured using modern automated exposure-adjusting cameras – without the special lens attachments [26]–[29]. These works utilize parametric models that can account for the nonuniform biasing of pixels that an image undergoes when a camera's exposure settings are automatically adjusted in response to the amount of light sensed. The exposure difference models utilized have been described in terms of comparametric functions [20] as well as by opto-electronic conversion functions (OECFs) [28], [29].

Along with the use of appropriate domain and range image models, another important factor to obtaining accurately registered images is that the procedure should have the ability to correct for (typically imperceptible) registration errors that exist among the adjacent images of a registered sequence; these are corrected by employing registration strategies that simultaneously account for all images in the sequence [10], [14]. These errors, when not accounted for, are most evident on mosaics created from sequences that loop back on themselves and can severely hinder applications involving, for example, superresolution [30].

In this paper, a framework is presented for optimally and simultaneously registering images while accounting for exposure differences. The need of such a framework is important for several reasons: (1) up to now, the issue of joint domain and range registration has only been approached utilizing pair-wise image registration [24]–[29], [31] – thus errors in the global mosaic have either not been correctable or have been corrected in a nonoptimal fashion, (2) it answers the question of how to generalize parametric range models to the case of multiple overlapping images [31], (3) it allows for the registration of sequences

Manuscript received January 30, 2003; revised July 23, 2003. The associate editor coordinating the review of this manuscript and approving it for publication was Dr. Bruno Carpentieri.

The author is with the Department of Electrical and Computer Engineering, Florida International University, Miami, FL. 33174 USA (e-mail: frank.candocia@fiu.edu).

Digital Object Identifier 10.1109/TIP.2003.819222

with severe exposure differences – this will be illustrated with two examples where it is shown that domain-only registration is not sufficient for the accurate registration of the sequences considered.

The procedure performs registration jointly in domain and range. It does so directly and globally. The direct approach utilizes the pixel values (in contrast to features) in the optimality criteria. The global approach is used as all pixels in an image are typically exposed by the same amount; consequently, the appropriate manner in which to determine the exposure-difference between images is to utilize all pixels common to the images' overlapping regions. Two domain models are utilized. The first consists of a translation and rotation model that is used in the initial stages of the registration. The second and actual model relating the domain transformations between images presented is the homographic (perspective) model. The range model employed makes use of one of Mann's comparametric functions. Its inclusion in the modeling is attractive as comparametric functions are theoretically well-founded, can be used to easily relate local exposure differences to a global coordinate reference and one only needs to estimate one parameter per image pair to quantify exposure differences between images in the sequence.

In the remainder of this paper, the registration approach is fully discussed. This begins in Section II by presenting the spatial coordinate and exposure-related transformations that are utilized in the paper. Section III details the optimization process and discusses the rationale behind it. Section IV provides a step-by-step description of the registration process as well as insights into algorithm specifics. This is then followed in Section V with experimental results on two image sequences and the paper concludes with a brief summary and conclusions in Section VI.

## II. Domain and Range Models

The registration approach of this paper relates the domain of an image function to those of other images by a homographic mapping. This model is known to describe the relation between perspective views captured by a pinhole camera that is allowed to pan, tilt, rotate and/or zoom about its optical center [12]. Equivalently, this model holds in relating images of planar surfaces under arbitrary camera motion. The homographic mapping has eight free parameters and is given by

$$\mathbf{p}(\mathbf{x}) = \frac{\mathbf{A}\mathbf{x} + \mathbf{b}}{\mathbf{c}^T\mathbf{x} + 1} \tag{1}$$

where $\mathbf{A} = [a_{11}, a_{12}; a_{21}, a_{22}]$ is a $2 \times 2$ scaling and rotation matrix, $\mathbf{b} = [b_1, b_2]^T$ is a $2 \times 1$ translation vector and $\mathbf{c} = [c_1, c_2]^T$ is a $2 \times 1$ "perspective" vector. The spatial coordinates are denoted by $\mathbf{x} = [x, y]^T$ and the superscript $T$ denotes vector transposition. Note that another domain mapping that will be used for initialization purposes considers pure rotation as well as translation. This is given by

$$\mathbf{p}(\mathbf{x}) = \begin{bmatrix} \cos\phi & \sin\phi \\ -\sin\phi & \cos\phi \end{bmatrix} \mathbf{x} + \mathbf{b} \tag{2}$$

and has only three parameters that need estimating: $\phi$, $b_1$ and $b_2$.

The registering of images in range as well as in domain can be important to accurate featureless registration methods; this is particularly true when capturing images with an automatic exposure-adjusting camera. This point will be emphasized through examples later in the paper. The range model used in this work corresponds to the "preferred" model of Mann [20]. The comparametric relation between the pixel values of two images $f(\mathbf{x})$ and $g(\mathbf{x})$, i.e., of two images of the same subject matter but that differ in exposure, for the "preferred" model[1] is

$$f(g; k) = \left[ \frac{\sqrt[c]{g}}{\sqrt[c]{g}(1 - k^a) + k^a} \right]^c \tag{3}$$

where $k$ is a scalar that quantifies the exposure difference between images $f$ and $g$, $a$ and $c$ are fixed camera parameters and the explicit dependence of $f$ and $g$ on $\mathbf{x}$ has been omitted for notational conciseness. For estimating the fixed camera parameters, the interested reader can refer to [20]. The "preferred" model is used herein because the author has conducted previous tests and determined this an acceptably good model for the camera that is used. Note that, given the above models, any image $g$ whose spatial coordinates and pixel values are transformed would yield a new image $f(g(\mathbf{p}(\mathbf{x})))$.

## III. Optimization Process

### A. Statistical Interpretation of the Image Set

The image sets in this paper consist of images of an arbitrary static scene under constant illumination conditions. That is, all objects in the scene are not moving and the light source (or sources if more than one) is not changing with time. Now, under the ideal and noiseless pinhole camera model, any 3-D point imaged under the constrained camera motion previously described would appear as having the same pixel value in any of the images captured in which it was contained. However, due to the presence of camera noise (electronically induced noise, spatial sampling, point spread function effects, lens distortion, quantization effects, etc.), there is uncertainty as to the true value of this pixel. As such, the scene being analyzed can be considered a stochastic process $G(\mathbf{x})$ for which our sequence of $N$ captured images $\{g_i(\mathbf{x}) | i = 1, \ldots, N\}$ constitutes a set of sample functions drawn from this process but which are related by a homographic mapping in domain and by a comparametric mapping in range.

Since both the domain and range models are parameterized, we will explicitly denote this by referring to the homographic mapping of (1), which is applied to image $i$, as $\mathbf{x}_i \equiv \mathbf{p}(\mathbf{x}; \boldsymbol{\theta}_i)$ where $\boldsymbol{\theta}_i = [a_{11}^i, a_{12}^i, a_{21}^i, a_{22}^i, b_1^i, b_2^i, c_1^i, c_2^i]^T$ is the vector containing all the parameters upon which this domain mapping depends. Similarly, the range mapping of (3), when applied to image $i$ and which is parameterized by $k_i$, will be denoted $f_i(\mathbf{x}) \equiv f(g_i(\mathbf{x}); k_i)$. Note that since parameters $a$ and $c$ are specific to a given camera and are thus fixed constants, we are not explicitly listing them in our notation. For all coordinates $\mathbf{x}$

[1]In Mann's paper, this equation is expressed as $g(f)$. To facilitate the implementation of this approach, the function $f$ has been expressed in terms of $g$ as we are mapping global coordinates into each image's local coordinate frame to determine which images are influencing the current global point under observation.

on a grid, we choose to minimize the variance of pixel values of any image contributing to the current point under analysis. The optimization procedure adjusts the parameters so that all images are registered, i.e., aligned, with respect to a reference image in both the domain and range of the image function.

Now, the set of $N$ images to register is $g_i(\mathbf{x})$ for $i = 1,\ldots,N$. Without loss of generality, let image $N$, i.e., $g_N(\mathbf{x})$, denote the reference image. Upon successful registration of the set of images, all images are related to the reference by

$$g_N(\mathbf{x}) = f_i(\mathbf{x}_i) = f(g_i(\mathbf{x}_i); k_i) \tag{4}$$

for all $i = 1,\ldots,N-1$ and where $\mathbf{x}_i$ is the vector of domain-mapped spatial coordinates of image $i$ and $f$ is the comparametric mapping which modifies the pixel values of $g_i$ according to the parameter $k_i$.

### B. Objective Function

In performing our registration, we wish to minimize the sum of the collective variances of pixel values at all spatial coordinates on our chosen grid. The objective function to minimize is thus

$$\begin{aligned} J(\boldsymbol{\alpha}) &= \sum_{\mathbf{x}} Var[G(\mathbf{x};\boldsymbol{\alpha})] \\ &= \sum_{\mathbf{x}} E\left[\left(G(\mathbf{x};\boldsymbol{\alpha}) - E[G(\mathbf{x};\boldsymbol{\alpha})]\right)^2\right] \end{aligned} \tag{5}$$

where $E[\cdot]$ and $Var[\cdot]$ are the statistical expectation and variance operators, respectively, and notice that $G(\mathbf{x};\boldsymbol{\alpha})$ is the random variable (from the stochastic process $G$) describing the pixel at location $\mathbf{x}$. The process is parameterized by vector $\boldsymbol{\alpha}$ because the sample functions, i.e., captured images $g_i(\mathbf{x})$, drawn from this process are known to be related by a domain and range mapping. Note that $\boldsymbol{\alpha} = [\boldsymbol{\theta}_1, k_1, \ldots, \boldsymbol{\theta}_{N-1}, k_{N-1}]^T$ is a vector of length $9(N-1)$ that consists of all domain mapping parameters $\theta_i$ and range mapping parameters $k_i$ for $i = 1,\ldots,N-1$. Also, the summation of (5) is a double summation over all sample points $(x, y)$ being considered. In the development that follows, it will be assumed without loss of generality, that image $N$ is the reference image. Making use of unbiased estimators for the mean and variance [32], we can approximate these two statistics with

$$\begin{aligned} \bar{G}(\mathbf{x};\boldsymbol{\alpha}) \equiv & E[G(\mathbf{x};\boldsymbol{\alpha})] \approx \frac{1}{M(\mathbf{x})}\left[\sum_{i=1}^{N} f(g_i(\mathbf{x}_i); k_i)\right] \\ = & \frac{1}{M(\mathbf{x})}\left[\sum_{i=1}^{N-1} f_i(\mathbf{x}_i)\right] \end{aligned} \tag{6}$$

and

$$\begin{aligned} Var[G(\mathbf{x};\boldsymbol{\alpha})] \approx & \frac{1}{M(\mathbf{x})-1}\left[\sum_{i=1}^{N}\left(f_i(g_i(\mathbf{x}_i); k_i)] - \bar{G}(\mathbf{x};\boldsymbol{\alpha})\right)^2\right] \\ = & \frac{1}{M(\mathbf{x})-1}\left[\sum_{i=1}^{N}\left(f_i(\mathbf{x}_i) - \bar{G}(\mathbf{x};\boldsymbol{\alpha})\right)^2\right] \end{aligned} \tag{7}$$

where $M(\mathbf{x})$ represents the number of images contributing a pixel value to sample point $\mathbf{x}$ in question. Please note that for any point $\mathbf{x}$, only those images contributing a value at this point are considered in the summation of (7) and that two or more images are needed to estimate the variance at this point; if a variance cannot be computed, then the point $\mathbf{x}$ under consideration does not contribute to the minimization of the cost in (5). Also, notice that ((6)–(7)) are in terms of $f_i(\mathbf{x}_i)$ as this is the parameterized version of the sample functions we have observed for which we must determine the appropriate domain and range mappings that properly registers our set of images.

Having established this notation, we can express (5) as

$$\begin{aligned} J(\boldsymbol{\alpha}) &= \sum_{\mathbf{x}} \frac{1}{M(\mathbf{x})-1}\left[\sum_{i=1}^{N}\left(f_i(\mathbf{x}_i) - \bar{G}(\mathbf{x};\boldsymbol{\alpha})\right)^2\right] \\ &= \sum_{\mathbf{x}}\sum_{i=1}^{N}\left[\frac{1}{\sqrt{M(\mathbf{x})-1}}\left(f_i(\mathbf{x}_i) - \bar{G}(\mathbf{x};\boldsymbol{\alpha})\right)\right]^2 \\ &= \sum_{\mathbf{x}}\sum_{i=1}^{N}\left[\frac{1}{\sqrt{M(\mathbf{x})-1}}\cdot\left(f_i(\mathbf{x}_i) - \frac{1}{M(\mathbf{x})}\cdot\sum_{j=1}^{N} f_j(\mathbf{x}_j)\right)\right]^2 \\ &= \sum_{\mathbf{x}}\sum_{i=1}^{N} e_i^2(\mathbf{x};\boldsymbol{\alpha}) \end{aligned} \tag{8}$$

where

$$e_i(\mathbf{x};\boldsymbol{\alpha}) = \frac{1}{\sqrt{M(\mathbf{x})-1}}\cdot\left[f_i(\mathbf{x}_i) - \frac{1}{M(\mathbf{x})}\sum_{j=1}^{N} f_j(\mathbf{x}_j)\right] \tag{9}$$

and recall that the parameters in $\boldsymbol{\alpha}$ are "embedded" in the domain mapping $\mathbf{x}_i$ and range mapping $f_i$.

The use of the variance as our objective optimality measure seems a natural one. First, since we know the images in our set are spatially related by the homographic transformation of (1) and tonally by the comparametric relation of (3) to a good accuracy, the only remaining source of error between the final set of registered images comes from camera-related noise. This type of noise is most commonly modeled as being independent and having zero-mean Gaussian statistics. With this in mind, there are only second-order statistic effects to account for. Further, notice that the variance measure in (5) being used over $N$ images defaults to the commonly used sum of squared errors when $N = 2$; this is known to yield the maximum likelihood (ML) solution. Thus, our optimality measure is akin to the ML parameter solution when multiple observations are available for each random variable (due to overlapping images) and indeed, defaults to the ML solution when $N = 2$. That is, given two images where one is the reference, the objective function becomes

$$\begin{aligned} J(\boldsymbol{\alpha}) &= \sum_{\mathbf{x}} e_1^2(\mathbf{x};\boldsymbol{\alpha}) + e_2^2(\mathbf{x};\boldsymbol{\alpha}) = \sum_{\mathbf{x}} 2\left[\frac{1}{2}\left(f_1(\mathbf{x}_1) - f_2(\mathbf{x}_2)\right)\right]^2 \\ &= \frac{1}{2}\sum_{\mathbf{x}}\left[f_1(\mathbf{x}_1) - f_2(\mathbf{x}_2)\right]^2 \end{aligned} \tag{10}$$

hence the minimization of the variance as the natural measure for parameter optimality. It is now noted that one of the error

measures that will be utilized later on is the average standard deviation. This is defined as

$$\bar{\sigma} \equiv \frac{1}{P} \sum_{\mathbf{x}} \sqrt{Var[G(\mathbf{x};\boldsymbol{\alpha})]} \tag{11}$$

where $P$ denotes the total number of points $\mathbf{x}$ that contributed to the sum.

### C. Iterative Solution

Since the cost function is nonlinearly related to the parameters in vector $\boldsymbol{\alpha}$, we require a nonlinear least squares approach to finding the parameters that minimize the objective function of (8). Here, we employ the Levenberg-Marquardt (LM) algorithm for performing our optimization [33]. A direct application of the LM procedure to the objective function in (8) yields a Hessian matrix $\mathbf{H}$ given by

$$\mathbf{H} = \sum_{\mathbf{x}} \sum_{i=1}^{N-1} \left[\nabla_{\boldsymbol{\alpha}} e_i(\mathbf{x};\boldsymbol{\alpha})\right]^T \left[\nabla_{\boldsymbol{\alpha}} e_i(\mathbf{x};\boldsymbol{\alpha})\right] \tag{12}$$

and an error-weighted gradient vector $\mathbf{g}$ which is

$$\mathbf{g} = -\sum_{\mathbf{x}} \sum_{i=1}^{N-1} e_i(\mathbf{x};\boldsymbol{\alpha}) \left[\nabla_{\boldsymbol{\alpha}} e_i(\mathbf{x};\boldsymbol{\alpha})\right]^T \tag{13}$$

where $e_i(\mathbf{x};\boldsymbol{\alpha})$ is as in (9) and its gradient is

$$\nabla_{\boldsymbol{\alpha}} e_i = \left[\frac{\partial e_i}{\partial \boldsymbol{\theta}_1}, \frac{\partial e_i}{\partial k_1}, \ldots, \frac{\partial e_i}{\partial \boldsymbol{\theta}_{N-1}}, \frac{\partial e_i}{\partial k_{N-1}}\right] \tag{14}$$

where the $\mathbf{x}$ and $\boldsymbol{\alpha}$ have been omitted for notational conciseness and, as previously mentioned, there are $N-1$ sets of domain and range parameters $\{\boldsymbol{\theta}_j, k_j\}$, $j = 1, \ldots, N-1$, to estimate given $N$ images because the chosen reference image stays fixed. Thus to evaluate (14) we must compute $\nabla_{\boldsymbol{\theta}_j} e_i$ and $\nabla_{k_j} e_i$ for $j = 1, \ldots, N-1$. We see that

$$\nabla_{\boldsymbol{\theta}_j} e_i = \frac{1}{\sqrt{M(\mathbf{x})-1}} \cdot \left[\nabla_{\boldsymbol{\theta}_j} f_i(\mathbf{x}_i) - \frac{1}{M(\mathbf{x})} \sum_{m=1}^{N} \nabla_{\boldsymbol{\theta}_j} f_m(\mathbf{x}_m)\right] \tag{15}$$

and

$$\nabla_{\boldsymbol{\theta}_j} f_i = \nabla_{\mathbf{x}_i} f_i \cdot \nabla_{\boldsymbol{\theta}_j} \mathbf{x}_i \tag{16}$$

where $\nabla_{\mathbf{x}_i} f_i$ is seen to be a $1 \times 2$ row vector and $\nabla_{\boldsymbol{\theta}_j} \mathbf{x}_i$ is a $2 \times 8$ matrix given the domain mapping of (1). We can further see, using (4), that

$$\nabla_{\mathbf{x}_i} f_i = \nabla_{g_i} f \cdot \nabla_{\mathbf{x}_i} g_i \tag{17}$$

where

$$\nabla_{g_i} f = \left[\frac{1}{\sqrt[c]{g_i}(1-k_i^a) + k_i^a}\right]^c \cdot \frac{k_i^a}{\sqrt[c]{g_i}(1-k_i^a) + k_i^a} \tag{18}$$

is a scalar and resulted from differentiating (3) and $\nabla_{\mathbf{x_i}} g_i = [\partial g_i/\partial x_i, \partial g_i/\partial y_i]$ is a $1 \times 2$ vector that contains the first derivative in the $x$ and $y$, i.e., row and column, directions of captured image $g_i$ which is to be evaluated at image sample $\mathbf{x}_i = [x_i, y_i]^T$. This first derivative of image $g_i$ is not truly known and must be approximated by, for example, a finite difference operation on pixel values near the sample point $\mathbf{x}_i$. The derivative operator employed yields an unbiased estimate and is given in [34].

For the homographic mapping, the second term in (16) results in

$$\begin{aligned}\nabla_{\boldsymbol{\theta}_j} \mathbf{x}_i &= \begin{bmatrix} \frac{\partial x_i}{\partial a_{11}^j} & \frac{\partial x_i}{\partial a_{12}^j} & \cdots & \frac{\partial x_i}{\partial c_2^j} \\ \frac{\partial y_i}{\partial a_{11}^j} & \frac{\partial y_i}{\partial a_{12}^j} & \cdots & \frac{\partial y_i}{\partial c_2^j} \end{bmatrix} \\ &= d_i(\mathbf{x}) \cdot \begin{bmatrix} x & y & 1 & 0 & 0 & 0 & -x \cdot x_i & -y \cdot x_i \\ 0 & 0 & 0 & x & y & 1 & -x \cdot y_i & -y \cdot y_i \end{bmatrix}\end{aligned} \tag{19}$$

if $i = j$. If $i \neq j$, $\nabla_{\boldsymbol{\theta}_j} \mathbf{x}_i$ is a matrix of zeroes of size $2 \times 8$. Note that $d_i(\mathbf{x}) = 1/(c_1^i x + c_2^i y + 1)$ and the definition of $\boldsymbol{\theta}_j$ in Section III-A was utilized in conjunction with the domain mapping of (1). Note that the mapping of (2), which is used for initialization purposes, would yield the $2 \times 3$ matrix

$$\nabla_{\boldsymbol{\theta}_j} \mathbf{x}_i = \begin{bmatrix} \frac{\partial x_i}{\partial \phi^j} & \frac{\partial x_i}{\partial b_1^j} & \frac{\partial x_i}{\partial b_2^j} \\ \frac{\partial y_i}{\partial \phi^j} & \frac{\partial y_i}{\partial b_1^j} & \frac{\partial y_i}{\partial b_2^j} \end{bmatrix} = \begin{bmatrix} -x\sin\phi + y\cos\phi & 1 & 0 \\ -x\cos\phi - y\sin\phi & 0 & 1 \end{bmatrix}. \tag{20}$$

The other gradient term that needed to be calculated was

$$\nabla_{k_j} e_i = \frac{1}{\sqrt{M(\mathbf{x})-1}} \cdot \left[\nabla_{k_j} f_i(\mathbf{x}_i) - \frac{1}{M(\mathbf{x})} \sum_{m=1}^{N} \nabla_{k_j} f_m(\mathbf{x}_m)\right] \tag{21}$$

where

$$\begin{aligned}\nabla_{k_j} f_i = \frac{\partial f}{\partial k_j} = -ac \left[\frac{\sqrt[c]{g_i}}{k_i^a\left(1 - \sqrt[c]{g_i}\right) + \sqrt[c]{g_i}}\right]^c \\ \cdot \left[\frac{k_i^a\left(1 - \sqrt[c]{g_i}\right)}{k_i\left(k_i^a\left(1 - \sqrt[c]{g_i}\right) + \sqrt[c]{g_i}\right)}\right]\end{aligned} \tag{22}$$

if $i = j$. If $i \neq j$, $\nabla_{k_j} f_i$ is a scalar with a value of zero. Equation (22) was arrived at by using the relations in (3) and (4).

## IV. Registration Steps

Because this is a nonlinear parameter optimization problem, the error surface defined by $J$ contains many local minima. Notice that, though there is no guarantee that the truly registered image set corresponds to the global minima of $J$ due to our finite set of noisy images, it is reasonable to expect that the registered set will have an error measure $J$ comparable to that of the global minima we seek. Therefore, as long as we begin our iterative scheme with an initial parameter set $\boldsymbol{\alpha}$ near the solution, we are likely to converge to an acceptable, if not optimal, solution.

To arrive at a solution, several steps are performed.

1) *Perform a pyramidal decomposition on each $g_i$.* An image pyramid can be created by simply averaging nonoverlapping $2 \times 2$ pixel blocks of the previous image level so that the resulting image is half the size of its predecessor in both its rows and columns [35]. The registration would proceed from the coarsest to the finest level of the pyramid and the transformations obtained at each pyramid level are used to initialize registration at the next finer level. This scheme is employed on the images of this

paper. The use of pyramids for registration has been previously well-justified [36].

2) *Low pass filter each image $g_i$*. The amount of filtering is a bit arbitrary but the purpose of this step is to mitigate the effects of noise as well as subdue image detail that is not relevant to the global registration sought. In general, a smoother signal will likely result in fewer local minima in the error surface that the algorithm can get trapped in. The most crucial stage of registration is at the coarsest level. In our scheme, the coarsest image is filtered more than at finer levels and the low pass filtering employed consisted of separable moving average (MA) filters [37].
3) *Pair-wise register the set of images*. Because it is easier to register two images than more than two, i.e., we require less computation and there are likely less local minima in $J$, we first perform pair-wise registration among the adjacent captured images.
    a) *Estimate the simultaneous translation, rotation and comparametric parameter $k$ between images*. At all levels except for the finest, we perform registration using the range model of (3) but, in domain, use the more restricted model of (2). At the coarsest level, all parameters are set to the identity transformation, i.e., the range parameter $k = 1$ and the domain model sets $\phi = 0$ and $\mathbf{b} = \mathbf{0}$. This estimate is refined as we process finer levels.
    b) *Estimate the homographic mapping between images*. At the finest level, we utilize the full domain and range models, namely, (1) and (3), respectively. The parameter estimates obtained from part a. serve to initialize the iterations of this last step. Note that, initially $\mathbf{c} = \mathbf{0}$ and $\mathbf{A} = [\cos\phi, \sin\phi; -\sin\phi, \cos\phi]$ where $\phi$ and $\mathbf{b}$ come from part a.
4) *Choose a reference image and perform the simultaneous registration of the set of images using the pair-wise estimates obtained from part 3*. Because the homographic and comparametric mapping constitutes a group structure, i.e., the functional composition of two homographic mappings results in a homographic mapping in domain and a range mapping in range, it is easy to convert the pair-wise mappings between adjacent images into how each image globally maps to the reference image [26]. This set of global mappings then constitutes the initial parameter vector $\boldsymbol{\alpha}$ for which to begin performing the optimization for simultaneously registering our image set. The global registration also proceeds in a pyramidal fashion. The initial vector $\boldsymbol{\alpha}$ begins the process at the coarsest level and is subsequently refined as we process finer levels.

Please note that these steps are not a recipe but only serve as a guide to achieving good simultaneous image registration performance. Alternate methods for creating image pyramids [35], [38] as well as filters to use [37] are available and when used, would supplant steps 1 and 2 above. However, the simple pyramid described above seems to work well in practice. The number of pyramid levels to utilize and the amount of filtering to perform is a bit subjective and typically requires tweaking as one must balance registration performance with speed of execution. Also, bilinear interpolation was used throughout the entire registration process when determining registration errors as it has experimentally been seen to be simple and effective. We have also used bicubic interpolation and not noticed any appreciable differences in performance.

## V. Experimental Results

Two image sequences are presented that illustrate the algorithm's performance and also provide examples of the benefits of simultaneous domain and range, i.e., joint, registration over domain-only registration when registering images that differ in exposure. All images were captured with a Sony DCRTRV30 camcorder and each image was resized to $240 \times 320$ pixels for the experiments in this paper. In both sequences, the camcorder roughly panned across a scene (from left to right) and then back again at a lower elevation. The camcorder was handheld and approximately moved about its optical center (though no great care was taken to achieve this) so that we could justify using the domain model of (1). Also, the camera used has been comparametrically modeled with the "preferred" model of (3) such that the fixed camera parameters used were $a = 0.64$, $c = 5.4$ and $k = \sqrt{2}$ for one exposure increment of the camera. Please note that the domain-only algorithm is identical to the joint algorithm except for the presence of the extra range parameter used in the joint registration.

The first set of images is illustrated in Fig. 1 and constitutes the "Parking Lot" sequence. In capturing these images, the exposure of the camera was manually reduced by one increment for each successive captured image. This results in a sequence of successively darker images for which the range parameter $k$ is known. Using the pyramidal approach described in the previous section, we pair-wise registered the images in the sequence first by using only the domain model and then by using the joint model. We utilized four pyramid levels and two-tap MA filters at all levels except the coarsest for which a four-tap MA filter was used. The registration time, error and the correlation coefficient between pairs of registered images appear in Table I under the respective "Pair-wise" sections of the table. Note that image pair 1 consists of images (a) and (b), image pair 2 consists of images (b) and (c), and so on. Also note that we are using the correlation coefficient $\rho$ [32] obtained from the images after performing pair-wise registration as a measure of registration accuracy. Given our assumption of images corrupted by additive Gaussian noise, this is an appropriate measure to utilize. We can see from the table that pair-wise domain-only registration performed as well as pair-wise joint registration as all $\rho$ values in both pair-wise cases are very similar and close to 1. [2] Notice that the average standard deviation $\bar{\sigma}$ between pair-wise registered image pixels is not as good an indicator to registration performance as is $\rho$. In the domain-only case, we see that $\bar{\sigma}$ was always greater than in the joint registration – sometimes more than twice greater. In general, the pair-wise registration

[2]We have noticed experimentally that values of $\rho > 0.95$ indicate a well-registered image – even though model mismatch and image noise typically result in small, visually imperceptible, registration errors.

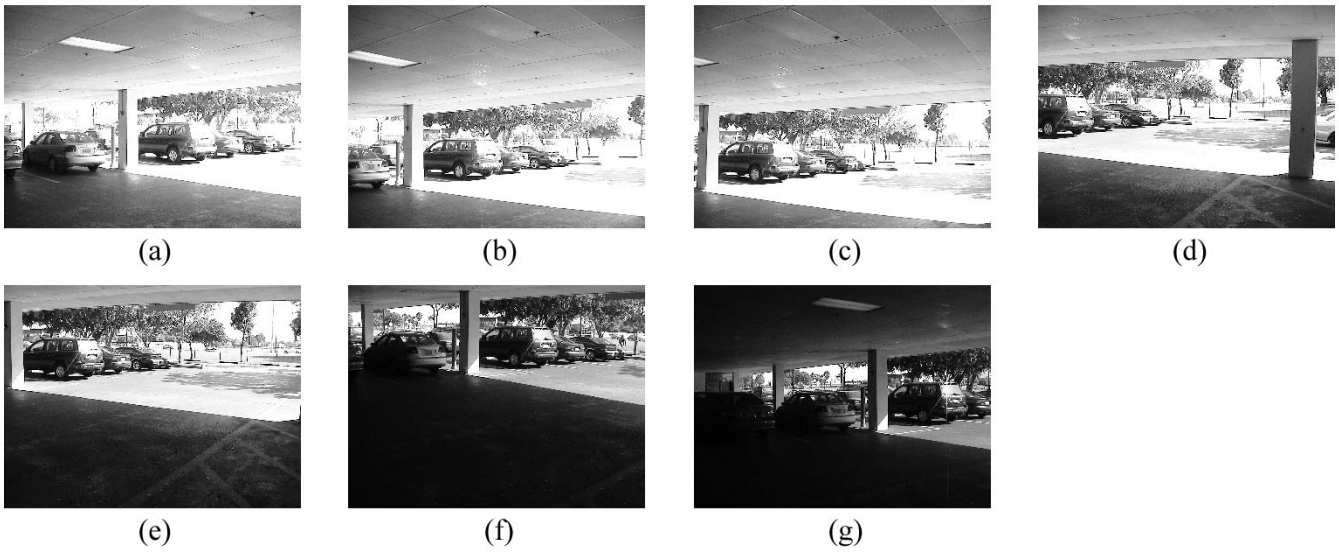


Fig. 1. "Parking Lot" image sequence. The images are 240 × 320 pixels in size.

TABLE I
REGISTRATION PERFORMANCE FOR "PARKING LOT" SEQUENCE

| | Domain Only Registration | | | | | Domain and Range Registration | | | | | | | |
|---|---|---|---|---|---|---|---|---|---|---|---|---|---|
| | Pair-wise | | | After Simultaneous | | Pair-wise | | | | | After Simultaneous | | |
| Pair | Time (s) | $\bar{\sigma}$ | ρ | $\bar{\sigma}$ | ρ | Time (s) | True $k$ | $\bar{\sigma}$ | ρ | Est. $k$ | $\bar{\sigma}$ | ρ | Est. $k$ |
| 1 | 18.3 | 11.7 | 0.976 | 23.9 | 0.659 | 45.8 | $\sqrt{2}$ | 5.6 | 0.977 | 1.54 | 14.48 | 0.921 | 0.95 |
| 2 | 19.8 | 8.2 | 0.978 | 16.8 | 0.851 | 35.3 | $\sqrt{2}$ | 5.0 | 0.978 | 1.34 | 8.2 | 0.948 | 1.63 |
| 3 | 23.3 | 16.5 | 0.949 | 17.0 | 0.892 | 32.6 | $\sqrt{2}$ | 8.0 | 0.951 | 1.96 | 8.3 | 0.945 | 2.03 |
| 4 | 19.9 | 12.7 | 0.978 | 13.2 | 0.967 | 36.0 | $\sqrt{2}$ | 7.7 | 0.979 | 1.47 | 8.1 | 0.976 | 1.42 |
| 5 | 21.3 | 15.4 | 0.973 | 19.5 | 0.902 | 32.1 | $\sqrt{2}$ | 8.7 | 0.974 | 1.65 | 10.9 | 0.941 | 1.45 |
| 6 | 23.5 | 11.2 | 0.960 | 27.2 | 0.666 | 43.1 | $\sqrt{2}$ | 7.6 | 0.961 | 1.47 | 8.4 | 0.940 | 1.42 |

time for the domain-only case was about 20 s in contrast to an average of about 37 s for the joint pair-wise registration. We can also notice that the range parameter $k$ was reasonably estimated during the joint pair-wise estimation, thus validating the use of our comparametric model. Any deviation from ideal values, i.e., $k = \sqrt{2}$ and $\rho = 1$, are due to the noisy images as well as mismatches in the comparametric model (model used and/or estimated intrinsic parameters) and domain model (particularly with the camera being hand-held). Please note that the algorithms were written and run using the Matlab 6.0 R12 package in the Windows 2000 environment on a Dell 330 Precision PC with a 1.5 GHz Pentium IV processor. Loop-intensive sections of the code were manually written in C and compiled as MEX files to help speed up the calculations.

Though the correlation coefficients from the pair-wise registration indicate good performance, the compounding effect of small registration errors (visually imperceptible from the pair-wise registration) is clearly present upon examining the "ghosting" effect on the second car from the left in both images of Fig. 2. To correct for this misalignment, we use these pair-wise estimates to initialize the simultaneous registration procedure. We used two pyramid levels to perform the simultaneous registration with three-tap MA filters at each level. The result of simultaneous joint registration is illustrated in the bottom image of Fig. 3. Notice in Table I that the obtained pair-wise transformations between images after the simultaneous registration still maintain high values of $\rho$, although they have slightly decreased (similarly the $\bar{\sigma}$ has increased). Examining $\rho$ for image pair 1 after the simultaneous joint registration we see a decrease from 0.977 to 0.921. This is attributed to comparametric model inaccuracies at high exposure differences. That is, during simultaneous joint registration, the significant exposure differences in the images of Fig. 1(a) and (g) result in an increase in range parameter error to compensate for this model mismatch. This compensation most affects those image pairs adjacent to images (1a) and (1g). Even with this comparametric model mismatch, we can see in Fig. 3 (bottom image) that the simultaneous joint registration has successfully corrected for the errors in the pair-wise transformations by removing the "ghosting" artifacts present in the pair-wise case. The simultaneous joint registration resulted in a global average pixel standard deviation of $\bar{\sigma} = 10.98$ and took 132 s to complete.

In contrast, attempting to correct for pair-wise errors using domain-only registration for the "Parking Lot" sequence is difficult at best. Because images (1a) and (1g) of Fig. 1 are so tonally different, the domain-only algorithm erroneously compensates for this pixel error by modifying the domain transformations of

Fig. 2. Comparison between pair-wise domain-only and pair-wise joint registration of the "Parking Lot" sequence. The reference image (in both domain and range) is that of Fig. 1(b). Notice the "ghosting" effect on the second car from the left resulting from the compounding of pair-wise registration errors in the domain-only case (top image) and the joint case (bottom image).

Fig. 3. Comparison between simultaneous domain-only and simultaneous joint registration. Both mosaics use Fig. 1(b) as the reference image. Using simultaneous domain-only registration to correct for pair-wise registration errors does not work because images Fig. 1(a) and (g) are so tonally different that the algorithm erroneously compensates for this by modifying the transformations of other images (top image). Only images (1a)-(1f) are shown here as (1g) was disproportionately distorted relative to the other images during the simultaneous registration. The simultaneous joint registration does not suffer from this effect and produces the correct registration (bottom image).

other images. This results in significant transformation errors specifically in images adjacent to (1a) and (1g) from Fig. 1. This is illustrated in the top image of Fig. 3 where severe "ghosting" is most noted in the car at the left as well as the light above it. Note that only images (1a)-(1f) in Fig. 1 are used in forming the top image as (1g) was badly distorted relative to these others. Lastly, a comparison of the tonal "quality" of the final joint and domain-only mosaics of the "Parking Lot" sequence in Figs. 2 and 3 shows that all objects in the joint mosaics are easily visible relative to when the domain-only mosaic is viewed. This is most evident when comparing objects on the left half of the domain-only mosaics that appear too dark to be clearly identified. Joint registration does not typically suffer from this as any object that has been multiply exposed can be readily viewed by specifying an appropriate exposure reference for the final mosaic.

The second set of images constitutes the "Office" sequence and is illustrated in Fig. 4. The camcorder is now operating in automated exposure-adjusting mode. This particular scene was chosen because the lighting in the interior of the office was much poorer relative to the lighting outside of the window. This creates a sequence of images for which the camera automatically increases the exposure setting to compensate for the poor lighting inside the office relative to when the camera is focused on the trees outside the window. As a result, it is difficult to identify objects inside the office in image (4e) of Fig. 4 but one can easily see the trees outside the window, whereas in image (4a), objects in the interior of the office are easily identifiable but the trees outside the window have been "washed out" due to the relative increased exposure setting at which it was captured. Again, pair-wise domain-only and joint registration is performed using the pyramidal approach of the previous section. Four pyramid levels and the same filters as with the "Parking Lot" sequence were utilized. The resulting registration performance is listed in Table II. As before, examining the correlation coefficients between pair-wise registered images indicates good registration accuracy in the case of joint registration as the smallest such value is $\rho = 0.971$. The average global standard deviation error after joint registration was $\bar{\sigma} = 9.3$ and the registration took 160 s to complete.

The domain-only registration yields some high $\rho$ values comparable to those of the joint registration and some poor ones too with image pairs 3, 6 and 7 having values less than 0.72. The pair-wise registration in these cases was visibly way-off. As

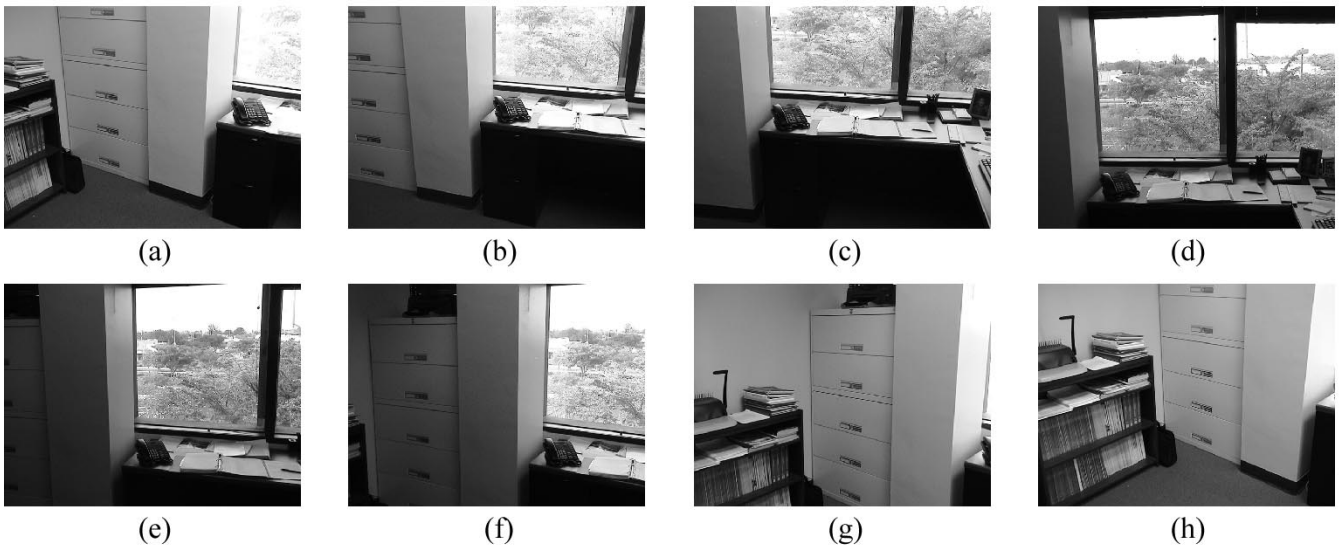


Fig. 4. "Office" image sequence. The images are 240 × 320 pixels in size.

TABLE II
REGISTRATION PERFORMANCE FOR "OFFICE" SEQUENCE

| | Domain Only Registration | | | Domain and Range Registration | | | | | | |
|---|---|---|---|---|---|---|---|---|---|---|
| | Pair-wise | | | Pair-wise | | | | After Simultaneous | | |
| Pair | Time (s) | $\bar{\sigma}$ | ρ | Time (s) | $\bar{\sigma}$ | ρ | Est. $k$ | $\bar{\sigma}$ | ρ | Est. $k$ |
| 1 | 9.1 | 18.3 | 0.916 | 33.9 | 5.8 | 0.994 | 1.82 | 8.2 | 0.987 | 1.56 |
| 2 | 18.3 | 14.7 | 0.974 | 29.9 | 8.3 | 0.990 | 1.87 | 9.0 | 0.990 | 1.62 |
| 3 | 12.9 | 37.9 | 0.573 | 42.9 | 11.4 | 0.971 | 2.65 | 12.0 | 0.964 | 2.57 |
| 4 | 18.5 | 6.5 | 0.965 | 33.8 | 6.1 | 0.978 | 0.86 | 6.5 | 0.977 | 0.92 |
| 5 | 14.7 | 17.3 | 0.962 | 30.5 | 5.8 | 0.989 | 0.48 | 6.2 | 0.984 | 0.58 |
| 6 | 7.7 | 33.0 | 0.693 | 32.9 | 5.2 | 0.986 | 0.25 | 5.2 | 0.985 | 0.26 |
| 7 | 13.8 | 23.3 | 0.720 | 21.7 | 3.7 | 0.990 | 0.55 | 4.9 | 0.986 | 0.59 |

such, the creation of a mosaic involving these grossly erroneous pair-wise transformations results in an image of little use and is thus not illustrated. It is important to now stress that performing simultaneous image registration requires good pair-wise registration accuracy as the transformations found are used to initialize the simultaneous procedure. Because the domain-only approach had pair-wise cases that were grossly in error, simultaneous registration cannot be performed and thus its exclusion from Table II in the domain-only case. We therefore, illustrate results for the joint registration procedure in Fig. 5. The top image is the mosaic formed from the joint pair-wise transformations. The reference image (in both domain and range) is that of Fig. 4(a). Here, again, is a case where small transformation errors are compounded and lead to misregistration that is most noticeable around the file cabinet toward the left part of the image. After simultaneous registration using two pyramid levels and three-tap MA filters, the mosaic at the bottom of Fig. 5 results. This image is now visually correct and examination of the pair-wise correlation coefficients after performing the simultaneous registration supports this claim. Even if we had been able to perform pair-wise domain registration, the small pair-wise errors would not have been fixed with simultaneous domain-only registration. Fig. 6 illustrates the final mosaic created using the simultaneous domain-only approach where the initial pair-wise transformations used to begin the process are the domain portion (those used in obtaining the bottom image of Fig. 5) of the simultaneous joint registration. Significant "ghosting" can be seen around the column between the file cabinet and desk illustrating again that the simultaneous domain-only procedure erroneously adjusts the domain transformations when large tonal differences between images exist. The reference image was (a) of Fig. 4.

One can notice some common themes upon examining the data of Tables I and II. The first is the use of the correlation coefficient as an indicator of goodness of registration and correspondingly, the average standard deviation as not as good an indicator. The second is that joint registration is typically about twice as slow as domain-only registration using the approach presented. The third is that after simultaneous registration, the correlation coefficient values usually drop and the average standard deviation usually increases. This is not surprising as the best computed pair-wise transformations do so based on noisy images and approximate domain and range transformation models. By using the simultaneous registration, there is a mechanism by which these errors can be optimally reduced in the context of the entire sequence. This means

Fig. 5. Comparison between pair-wise and simultaneous joint registration of the "Office" sequence. The domain and range reference is the image in Fig. 4(a). Pair-wise registration results in misalignment noticeable around the file cabinet (top image) while simultaneous registration results in correct image alignment (bottom image).

Fig. 6. Demonstration of inappropriateness of simultaneous domain-only registration on the "Office" sequence. Because domain-only registration was not capable of supplying reasonably accurate pair-wise transformations to use in simultaneous registration, the sequence was initialized with the domain transformations obtained from the simultaneous joint registration (those used in creating the bottom image of Fig. 5). Even so, the lack of exposure modeling illustrates that large tonal differences between images severely affects the simultaneous domain-only registration's ability to account for such differences as "ghosting" is visibly clear around the file cabinet and the column adjacent to it. The reference image is that of Fig. 4(a).

trading-off pair-wise registration accuracy in favor of global registration accuracy.

## VI. Summary and Conclusions

An approach to the featureless simultaneous registration of images has been presented which does so optimally in both the domain and range of the images considered. The procedure is particularly useful on automated exposure-adjusted images to correct for small pair-wise registration errors that, if not corrected, typically result in ghosting artifacts when a mosaic is created. This is typically evident when working with image sequences that loop back on themselves. Examples of two sequences exhibiting significant exposure differences were used to demonstrate that joint registration is necessary in order to obtain accurate registration results. Since joint registration can more than double the registration time, it should be used when the option of domain-only registration is inadequate. This will usually be the case when an image sequence loops back on itself and significant tonal differences between images in the sequence exists. A drawback of this method is that simultaneous registration times significantly rise as the number of images in the sequence increases. This is due to the large number of parameters required to be simultaneously estimated, i.e., $9(\mathrm{N}-1)$ where $\mathrm{N}$ denotes the number of images in the sequence, and, in particular, is also due to the computing of the Hessian matrix after each iteration of the LM procedure.

## Acknowledgment

The author would like to thank the anonymous reviewers for providing helpful comments and suggestions that were used in preparing the final manuscript.

## References

[1] R. Szeliski, "Video mosaics for virtual environments," *IEEE Computer Graphics and Applications*, vol. 16, no. 2, pp. 22–30, 1996.
[2] ——, "Image Mosaicing for Tele-Reality Applications," Digital Equipment Corp, Cambridge Research Lab, CRL 94/2, 1994.
[3] E. M. Mikhail, J. S. Bethel, and J. C. McGlone, *Introduction to Modern Photogrammetry*. New York: Wiley, 2001.
[4] J. B. A. Maintz and M. A. Viergever, "A survey of medical image registration," *Med. Imag. Anal.*, vol. 2, no. 1, pp. 1–37, 1998.
[5] M. C. Chiang and T. E. Boult, "Efficient image warping and super-resolution," in *Proc. IEEE Workshop on Applications of Computer Vision (WACV' 96)*, 1996, pp. 56–61.
[6] U. R. Dhond and J. K. Aggarwal, "Structure from stereo – A review," *IEEE Trans. Syst., Man, Cybern.*, vol. 19, no. 6, pp. 1489–1510, 1989.
[7] H. S. Sawhney and S. Ayer, "Compact representation of videos through dominant multiple motion estimation," *IEEE Trans. Pattern Anal. Machine Intell.*, vol. 18, no. 8, pp. 814–830, 1996.
[8] M. Irani, S. Hsu, and P. Anandan, "Video compression using mosaic representations," *Signal Process.: Image Commun.*, vol. 7, pp. 529–552, 1995.
[9] L. G. Brown, "A survey of image registration techniques," *ACM Comput. Surv.*, vol. 24, no. 4, pp. 325–376, Dec. 1992.
[10] H. Y. Shum and R. Szeliski, "Systems and experiment paper: Construction of panoramic image mosaics with global and local alignment," *Int. J. Comput. Vis.*, vol. 36, no. 2, pp. 101–130, 2000.
[11] M. Irani and S. Peleg, "Improving resolution by image registration," *Comput. Vis., Graph., Image Process.: Graph. Models Image Process.*, vol. 53, no. 3, pp. 231–239, 1991.
[12] S. Mann and R. Picard, "Video orbits of the projective group: A simple approach to featureless estimation of parameters," *IEEE Trans. Image Processing*, vol. 6, pp. 1281–1295, Sept. 1997.
[13] S. Baker and T. Kanade, "Superresolution Optical Flow," Robotics Institute, Carnegie Mellon Univ., Pittsburgh, PA, CMU-RI-TR-99–36, 1999.
[14] H. S. Sawhney and R. Kumar, "True multi-image alignment and its applications to mosaicing and lens distortion correction," *IEEE Trans. Pattern Anal. Machine Intell.*, vol. 21, pp. 235–243, Mar. 1999.
[15] M. Irani and P. Anandan, "All about direct methods," in *Proc. Int. Workshop Vision Algorithms*, 1999, pp. 267–277.
[16] P. Torr and A. Zisserman, "Feature based methods for structure and motion estimation," in *Proc. Int. Workshop on Vision Algorithms*, 1999, pp. 278–295.

[17] S. Mann and R. W. Picard, "On being 'undigital' with digital cameras: Extending dynamic range by combining differently exposed pictures," in *Proc. of IS&T 48th Annual Conference*, May 1995, pp. 422–428.
[18] P. E. Debevec and J. Malik, "Recovering high dynamic range radiance maps from photographs," in *Proc. SIGGRAPH*, 1997, pp. 369–378.
[19] T. Mitsunaga and S. Nayar, "Radiometric self calibration," *Proc. IEEE Conf. Computer Vision and Pattern Recognition*, pp. 374–380, 1999.
[20] S. Mann, "Comparametric equations with practical applications in quantigraphic image processing," *IEEE Trans. Image Processing*, vol. 9, pp. 1389–1406, Aug. 2000.
[21] S. Mann and R. Mann, "Quantigraphic imaging: Estimating the camera response and exposures from differently exposed images," in *Proc. IEEE Conf. Computer Vision and Pattern Recognition*, 2001, pp. 842–849.
[22] R. Fattal, D. Lischinski, and M. Werman, "Gradient domain high dynamic range compression," *ACM Trans. Graph.*, vol. 21, no. 3, pp. 249–256, 2002.
[23] S. K. Nayar and T. Mitsunaga, "High dynamic range imaging: Spatially varying pixel exposures," in *IEEE Conf. Computer Vision and Pattern Recognition*, vol. 1, June 2000, pp. 472–479.
[24] Y. Y. Schechner and S. K. Nayar, "Generalized mosaicing," *Proc. IEEE Conf. Computer Vision and Pattern Recognition*, vol. 1, pp. 17–24, 2001.
[25] M. Aggarwal and N. Ahuja, "High dynamic range panoramic imaging," in *Proc. IEEE Int. Conf. Computer Vision*, vol. 1, 2001, pp. 2–9.
[26] S. Mann, "'Pencigraphy' with AGC: Joint parameter estimation in both domain and range of functions in same orbit of the projective-wyckoff group," in *IEEE Int. Conf. Image Processing (ICIP '96)*, vol. 3, Los Alamitos, CA, 1996, pp. 193–196.
[27] F. M. Candocia, "Jointly registering images in domain and range by piecewise linear comparametric analysis," *IEEE Trans. Image Processing*, vol. 12, pp. 409–419, Apr. 2003.
[28] D. Hasler and S. Susstrunk, "Color handling in panoramic photography," in *Proc. IS&T/SPIE Electronic Imaging 2001: Videometrics and Optical Methods for 3D Shape Measurements*, vol. 4309, 2001, pp. 62–72.
[29] ——, "Modeling the opto-electronic conversion function (OECF) for application in the stitching of panoramic images," in *Proc. ICIS*, 2002, pp. 379–380.
[30] D. Capel and A. Zisserman, "Computer vision applied to super resolution," *IEEE Signal Processing Mag.*, vol. 20, no. 3, pp. 75–86, 2003.
[31] M. Uyttendaele, A. Eden, and R. Szeliski, "Eliminating ghosting and exposure artifacts in image mosaics," *Proc. IEEE Int. Conf. Computer Vision and Pattern Recognition (CVPR)*, vol. II, pp. 509–516, 2001.
[32] A. Papoulis and S. U. Pillai, *Probability, Random Variables and Stochastic Processes*, 4th ed. New York: McGraw Hill, 2002.
[33] W. H. Press *et al.*, *Numerical Recipes in C*, 2nd ed: Cambridge Univ. Press, 1992.
[34] B. K. P. Horn, *Robot Vision*. New York: McGraw-Hill, 1986, p. 164.
[35] K. R. Castleman, *Digital Image Processing*. Englewood Cliffs, NJ: Prentice-Hall, 1996.
[36] J. R. Bergen, P. Anandan, K. J. Hanna, and R. Hingorani, "Hierarchical model-based motion estimation," in *Proc. 2nd Eur. Conf. Computer Vision (ECCV)*, 1992, pp. 237–252.
[37] A. V. Oppenheim and R. W. Schafer, *Discrete Time Signal Processing*. Englewood Cliffs, NJ: Prentice-Hall, 1989.
[38] P. J. Burt and E. H. Adelson, "The Laplacian pyramid as a compact image code," *IEEE Trans. Commun.*, vol. COM-31, no. 4, pp. 532–540, 1983.

**Frank M. Candocia** (M'94) received the B.S. and M.S. degrees in electrical engineering in 1991 and 1993, respectively, from Florida International University, Miami. In 1998, he received the Ph.D. degree in electrical and computer engineering from the University of Florida, Gainesville, where his work focused on learned optical image superresolution. During his doctoral studies, he also investigated superresolution of synthetic aperture radar imagery at MIT Lincoln Labs.

From 1998 to 2000, he was a Senior Systems Engineer for the Raytheon Systems Company, Bedford, MA, where he was responsible for the design and implementation of the search and acquisition portion of the National Missile Defense program's X-band radar. He is currently an Assistant Professor with the Department of Electrical and Computer Engineering at Florida International University and is the founder of the Image Understanding Lab (http://iul.eng.fiu.edu). His research interests include all phases of the image understanding problem as well as the tools needed toward their eventual solution.

Dr. Candocia has been the recipient of several scholarships and fellowships including a University of Florida Graduate Minority Fellowship and a Motorola Fellowship.